

High-resolution proglacial lake records of pre-Little Ice Age glacier advance, northeast Greenland

KATHRYN ADAMSON, TIMOTHY LANE, MATTHEW CARNEY, THOMAS BISHOP, CATHY DELANEY

Adamson, K., Lane, T.P., Carney, M., Bishop, T., & Delaney, C.: High-resolution proglacial lake records of pre-Little Ice Age glacier advance, northeast Greenland

Understanding Arctic glacier sensitivity is key to predicting future response to air temperature rise. Previous studies have used proglacial lake sediment records to reconstruct Holocene glacier advance-retreat patterns in South and West Greenland, but high-resolution glacier records from High Arctic Greenland are scarce, despite the sensitivity of this region to future climate change. Detailed geochemical analysis of proglacial lake sediments close to Zackenberg, northeast Greenland, provides the first high-resolution record of Late Holocene High Arctic glacier behaviour. Three phases of glacier advance have occurred in the last 2000 years. The first two phases (c. 1320-800 cal. a BP) occurred prior to the Little Ice Age (LIA), and correspond to the Dark Ages Cold Period and the Medieval Climate Anomaly. The third phase (c. 700 cal. a BP), representing a smaller scale glacier oscillation, is associated with the onset of the LIA. Our results are consistent with recent evidence of pre-LIA glacier advance in other parts of the Arctic, including South and West Greenland, Svalbard, and Canada. The sub-millennial glacier fluctuations identified in the Madsen Lake succession are not preserved in the moraine record. Importantly, coupled XRF and XRD analysis has effectively identified a phase of ice advance that is not visible by sedimentology alone. This highlights the value of high-resolution geochemical analysis of lake sediments to establish rapid glacier advance-retreat patterns, in regions where chronological and morphostratigraphical control is limited.

26 Kathryn Adamson (k.adamson@mmu.ac.uk), Matthew Carney, and Cathy Delaney, School of Science
27 and the Environment, Manchester Metropolitan University, Manchester, M1 5GD, UK; Timothy Lane,
28 School of Natural Sciences and Psychology, Liverpool John Moores University, Liverpool, L3 3AF, UK;
29 Thomas Bishop, Department of Geography, The University of Manchester, Manchester, M13 9PL, UK.
30

Unprecedented Arctic air temperature rise is causing profound retreat of the Greenland Ice Sheet (GrIS) and its surrounding glaciers and ice caps (GIC). Recent mapping has shown that GICs cover 90000 km², an area 50% larger than previously estimated (Rastner *et al.* 2012). Although this represents only 5% of Greenland's glaciated area (Wouters *et al.* 2017), it accounts for 15-20% of Greenland's eustatic sea level rise contribution (~ 0.05 - 1.10 mm a⁻¹ from 2003-2008, Bolch *et al.* 2013). The small size of these ice masses means that they are more sensitive to climate change than the GrIS (Machguth *et al.* 2013). This is especially significant in the High Arctic (north of the +6 °C July isotherm; Bliss 1997), which is expected to experience some of the most intense changes in response to climate warming by the end of the century, including enhanced glacier melt and increased precipitation (Lund *et al.* 2017). These changes are expected to be spatially and temporally non-uniform (e.g. Carr *et al.* 2013; Moon *et al.* 2014), so understanding the rate and pattern of sub-centennial glacier behaviour is important to reliably predict future changes.

Of the 20 available mass balance records from GICs, multi-decadal measurements are scarce. Where they do exist (see Machguth *et al.* 2016 for locations), they rarely extend to the present day or are not annually resolved. One record, from the Nuusuaq glaciers in West Greenland (1892-1993) spans 101 years, and data from Mittivakkat, southeast Greenland, spans 20 years (1996-present). In northeast Greenland, two detailed records exist (2008-present) at A. P. Olsen ice cap and Freya glacier, close to Zackenberg (Machguth *et al.* 2013, 2016), but these do not yet provide multi-decadal archives. In some locations, such as southeast Greenland, air photographs have been valuable in examining decadal changes in glacier fluctuations (e.g. Bjørk *et al.* 2012) and enhancing the resolution of the historical, monitored, record. Mass balance estimates generated from downscaled regional climate models can also be used to bridge gaps in the data (Noël *et al.* 2018). However, in both of these cases their spatial and temporal resolution often remains too low to reliably identify decadal and centennial GIC change. It is only through high-resolution analysis of Holocene glacier records that sub-millennial glacier variability can be robustly resolved.

57

58 The majority of Holocene GIC records are derived from West, South, and southeast Greenland
59 (Table 1), and show asynchronous and asymmetrical glacier dynamics over the last few millennia in
60 response to climatic and aclimatic forcing (e.g. Balascio *et al.* 2015; Böning *et al.* 2016; Abermann *et*
61 *al.* 2017; Vieli *et al.* 2017). Reconstructions of Late Holocene ice cap and mountain glacier behaviour
62 in Greenland are frequently based on terrestrial cosmogenic nuclide dating of moraines (e.g. Young *et*
63 *al.* 2015; Jomelli *et al.* 2016). However, sub-millennial glacier advance-retreat patterns are rarely well-
64 preserved in the moraine record, making it difficult to reliably identify the drivers of glacier behaviour
65 (Balascio *et al.* 2015).

66

67 Unlike the geomorphological record, proglacial lakes can record continuous, high-frequency,
68 sub-millennial, changes in glacier behaviour that can be radiocarbon dated, providing important
69 context for present day and future glacier retreat. Glacier-fed lake basins record variations in fine
70 grained (silt and clay) minerogenic sediment production resulting from glacier response to climate
71 changes (Kárlén 1981; Carrivick & Tweed 2013). Increased glacier activity (sustained advance or
72 retreat) leads to enhanced subglacial bedrock erosion, and a subsequent increase in sediment delivery
73 to lake basins downstream (Leeman & Niessan 1994; Palmer *et al.* 2010; McGregor *et al.* 2011;
74 Striberger *et al.* 2011). Depending on the bedrock mineralogical composition, increases or decreases
75 in specific minerals in the lake record can therefore be used as a proxy for glacier activity.

76

77 High-resolution mineral analysis of proglacial lake sediments has been used to reconstruct
78 sub-millennial Holocene glacier advance-retreat patterns and catchment change in Norway (Bakke *et*
79 *al.* 2013), Svalbard (Gjerde *et al.* 2017; de Wet *et al.* 2018), and southeast Greenland (Balascio *et al.*
80 2015), but highly resolved proglacial lake records are scarce in High Arctic Greenland. Instead, existing
81 studies in this region focus on palaeoecological analysis of full Holocene sequences to reconstruct local
82 and regional climate change (e.g. Wagner *et al.* 2000; Klug *et al.* 2009a, b; Schmidt *et al.* 2011; Bennike

& Wagner, 2012; Axford *et al.* 2017; Lasher *et al.* 2017;), and glacier and ice sheet fluctuations are not directly examined. Using detailed geochemical analysis of proglacial lake sediments, we present the first high-resolution record of Late Holocene glacier behaviour in this part of High Arctic Greenland (74° N).

Study setting

Geological setting

Zackenberglies on Wollaston Foreland in High Arctic northeast Greenland (74 – 75° N), ~ 50 km east of the GrIS (Fig. 1A). The region is characterised by wide valleys and steep sided plateaux and is bound by Lindeman Fjord and Tyrolerfjord to the north and south, respectively. A geological flexure and thrust zone in Zackenbergdalen (74.47° N, 20.57° W) separates Cretaceous sandstones and Tertiary basalts to the east, and Caledonian gneiss to the west. The bedrock adjacent to, and likely underlying the study ice cap, Slettebreen (Fig. 1), is dominantly Proterozoic orthogneiss, with some Proterozoic or Ordovician pelitic, semi-pelitic, and psammitic metasediments (Pedersen *et al.* 2013). It is not currently possible to further resolve the spatial distribution of catchment geology, due to present-day ice coverage, but our analysis shows that local lithologies are rich in silica (Si), Iron (Fe), Potassium (K), Calcium (Ca), and Aluminium (Al) (see Results).

Climatic setting

The regional climate is conditioned by the cold East Greenland current. This part of Greenland has a typical High Arctic climate, with mean annual air temperature of -9 °C (annual range: ~ -24.5 to 6.6 °C), based on 1996-2015 values measured at Zackenberg Research Base, 19 km from the study site (Hobbie *et al.* 2017). Summer (JJA) air temperatures average 4.5 °C (Hobbie *et al.* 2017), and precipitation (~ 200 mm a⁻¹) falls predominately as snow from September to May, and rain and/or snow from June to August (Hansen *et al.* 2008). Rivers close to Zackenberg typically flow from June-September, and sea

ice persists from October to May. The region is underlain by continuous permafrost with a 20-100 cm thick active layer (Christiansen *et al.* 2008, Christoffersen *et al.* 2008; Hansen *et al.* 2015).

Glacial history and geomorphology

High elevation erratics, trimlines, and moraines have been reported up to 500 m above sea level (a.s.l.) in the Store Søndal and Zackenberg valleys (Bretz 1935; Christiansen & Humlum 1993), suggesting that outlet glaciers from the GrIS and local ice caps previously extended into major valleys and fjords, and reached the shelf edge (Bennike & Weidick 2001; Ó Cofaigh *et al.* 2004; Evans *et al.* 2009). Regional deglaciation began after the Last Glacial Maximum (LGM) and continued through the Holocene. Zackenberg valley became ice-free between 13000 and 11000 years ago (Gilbert *et al.* 2017), but the time by which glaciers reached their present position is currently unknown.

Slettebreen ice cap and study catchment

Slettebreen (~ 17 km²) is largely confined to an upland plateau (1200 m a.s.l.) and is drained by six outlet glaciers to the south and east, and one to the north that extends to 450 m a.s.l and displays evidence of surge activity (periodic increases in flow speeds unrelated to external triggers; Meier & Post 1969; Sharp 1988). Large, undated, moraines beyond the present-day ice margins indicate that Slettebreen's outlet glaciers previously extended radially, towards Slettedalen, Storesødal, and Lindeman Fjord. Based on the established area–altitude balance ratio (AABR) method (Rea 2009) Slettedalen's current equilibrium line altitude (ELA) is estimated at 1071 - 1081 m a.s.l. (AABRs of 1.67 to 2.0).

The study lake (74.58° N, 21.07° W, 504 m a.s.l.), previously unnamed and hereafter referred to as Madsen Lake (area = 0.04 km², depth = 2 m), occupies a steep sided over-deepened basin ~ 1.6 km from the eastern margins of Slettebreen, and is fed by three small outlet glaciers (Figs 1A, B, 2) that currently terminate on the flanks of the plateau, ~ 0.8 – 1.5 km from the plateau edge. The lake

catchment contains ice moulded bedrock, unconsolidated glacial, glaciofluvial, and colluvial sediment, and sparse tundra vegetation. The small catchment area and proximity to the margins of Slettebreen, means that sediment storage between the glacier and lake is limited, non-glacial sediment input is minimised, and the basin provides a reliable record of glacier behaviour.

Based on morphostratigraphic similarities with other Greenlandic basins (Weidick 1968; Kelly & Lowell 2009), and the freshness of landforms, two moraine positions are identified in the Madsen Lake basin. Position 1 is a large, undated, moraine complex downstream of the lake, thought to correspond to a period of still-stand during retreat from the LGM position (Fig. 1B). Position 2, upstream of the lake, is a complex of moraine ridges thought to correspond to the most recent phase of glacier advance during the Late Holocene, possibly associated with the Little Ice Age (LIA), and suggests that the Madsen Lake basin was not overridden by ice at that time. Given the knowledge of Greenlandic glacier behaviour during this period (Kelly & Lowell 2009), it is likely that Position 2 moraines formed during a regrowth of ice, following the Holocene Thermal Maximum. The reconstructed palaeo-ELAs (AABRs 1.67 to 2.0) at Moraine Positions 1 and 2 are 761 - 784 m a.s.l. and 959 - 975 m a.s.l., respectively.

Methods

Lake sediment coring

Lake cores were taken in spring (May), when the surface of Madsen Lake was frozen. Suitable coring locations were established using aerial photographs, satellite imagery, and ArcticDEM data, which identified a deep central lake basin and shallower rim. Samples were taken from the deepest part of the central basin, to avoid reworked sediment or sediment gravity flows. Cores were obtained using a Russian-type corer, capturing the water-sediment interface and extending to a maximum sediment depth of 80 cm, before striking bedrock or boulders. The core was sub-sampled with a scalpel in the field at 1.0 and 0.5 cm resolution, depending on water content.

Laboratory analysis

Sediment grain size was measured using a Malvern Mastersizer 2000 and Hydro 2000G liquid handling unit, with triplicate measurements and bracketing cleaning cycles. Prior to analysis, organic matter was removed using 40% hydrogen peroxide, and samples were dispersed in sodium hexametaphosphate solution. Particle size distribution was modelled using a Mie Theory estimation model configured for silica sand, which is particularly effective for grains <10 µm, such as the fine-grained Madsen Lake sediments. Particle size analysis (PSA) was used to calculate GSD90, the 90th percentile of grain size distribution.

Samples were freeze-dried prior to elemental, mineralogical, magnetic, and carbon analysis and pressed (at 3.5 n kg⁻¹) into Chemplex 1330 sample holders with a 4 µm Mylar film window. Sediment elemental composition (X-Ray Fluorescence, XRF) was analysed using a Rigaku NEX-CG with an RPF-SQX scattered ray FP method (Helium-purged). This system uses a 'Rigaku Profiling Fitting-Spectra Quant X' algorithm to provide elemental mass estimates. Sample mineralogy (X-ray powder diffraction data, XRD) was collected using a PANalytical X'Pert diffractometer fitted with a PixCEL 1-D detector using a Cu anode ($\lambda = 0.5406 \text{ \AA}$) with the generator set at 40 mA, 40 kV. Samples were prepared as flat powder and collected in transmission geometry in the range 5-120° 2θ with a step size of 0.013° 2θ and a collection time of 118 sec. step⁻¹ using automatic divergence and antiscatter slits with an observed length of 8.0 mm. Data were processed using HighScore Plus version 4.0.

Eight clasts from Slettedalen were crushed and analysed for elemental (XRF) and mineralogical (XRD) composition. Pebbles were selected in the field on the basis that they are representative of local bedrock lithologies, delivered from meltwater streams draining Slettebreen, and can be used to compare to lake sediment geochemical signatures.

A Bartington MS2B sensor and MS3 interface were used to measure sediment magnetic susceptibility (MS) at high frequency (χ_{hf}). Corrections for sample volume follow Dearing *et al.* (1999). MS is a relative measure of the magnetisation of minerals, and in a sedimentary sequence can be influenced by factors including changes in clastic sediment content, erosion of different source rocks, and time-dependent weathering.

Total organic carbon (TOC) was measured using a Shimadzu TOC-VSSI analyser, with ~ 40 mg of freeze-dried sediment in crucibles capped with inert glass wool. Samples were analysed according to machine standard protocols for sediment samples, and 10 mg glucose standard. 20 random samples from the core succession were tested for inorganic carbon, and all yielded results below detection limits.

Statistical analysis

Principle component analysis (PCA), which establishes the leading mode of data variability (expressed as the first component), was performed using 10 elements from the XRF data selected on the basis of abundance in the lake sediments and bedrock clast samples (Al, K, Ca, Rb, Ti, Fe, Si, Mg, Mn, and Sr). Data were centre-log-ratio transformed, and two outlier samples at (42.0-43.0 and 60.5-61.0 cm) were removed. Analysis was performed in R v.3.4.2 (R Core Team 2017) and transformed using the chemometrics v.0.1 package (Filzmoser & Varmuza 2017).

Cluster analysis of the XRD data was used to examine the mineralogical signatures of the sedimentary units, to provide additional detail to the elemental composition (XRF), and thus test for fundamental differences between depositional phases. HighScore Plus (v. 4.0) used diffraction peak position and profile as the data source, and position and intensity (as a measure of crystalline concentrations) as the comparison criteria. Cluster assignments were validated by Fuzzy Clustering, which assigns each dataset to a parent cluster based on a figure of merit, which is indicative of the

strength and reliability of cluster assignments. This method is especially beneficial as it enables datasets to be evaluated within multiple clusters to yield the most appropriate cluster assignments. Relative intensity of the diffraction peaks was used to calculate the relative abundance of dominant minerals within each cluster.

Core chronology

The lake core chronology is based on four radiocarbon (^{14}C) ages of *in-situ* organic macrofossils (undifferentiated bryophytes) taken from individual laminae, avoiding sampling across multiple laminations; samples were analysed at Beta Analytic (Table 1). Calibration and age-depth modelling was performed in Bacon v.2.3.3 (Blaauw & Christen 2011) using the IntCal13 (Reimer *et al.* 2013) radiocarbon calibration curve. The Bacon algorithm is a Bayesian approach to accumulation rate modelling and the default parameters were used throughout.

Results

Catchment lithology and geochemistry

Eight clast samples represent five lithological categories: quartz, gneiss, granite, unakite, and sandstone. XRF data show that all clasts are rich in Si (typically 22.4-32.0 mass %) as well as Al, Ca, Fe, Na, Ti, and Mg (Table 4). The high concentrations of these minerals make them suitable for tracking glacial erosion, and they have therefore been selected for use in this study. Other elements such as Rh, P, Zr, Mn, Sr, Rb, and Ba are present in lower abundance (typically 0.5-0.02 mass %). XRD analysis indicates that the dominant mineral constituents include quartz, biotite, orthoclase, and epidote. The clast elemental composition and mineral signatures are reflected in the lake sedimentary succession, described below.

Lake stratigraphy and sediment characteristics

Five stratigraphic units have been identified based on sedimentology, physical characteristics (particle size, dry bulk density (DBD), TOC (indicator of organic matter), and MS (a relative indicator of clastic sediment composition), Table 3), and geochemistry (XRF and XRD). Figure 3 focuses on selected elements present in the lake sediments and local bedrock (Table 4), and their ratios, which fluctuate according to the sequence stratigraphy. On this basis, elemental signatures are used as proxies for glacier behaviour and lake basin conditions. Ti and Ti/Al ratios are indicators of detrital clastic sediment input and associated glacier activity, consistent with local lithologies and ratios, and used elsewhere (e.g. Bakke *et al.* 2009, 2013). Rb/Sr ratios are used as an indicator of chemical weathering within the lake catchment (e.g. Vasskog *et al.* 2011), as Sr, which has an affinity with Ca, is easily released during chemical weathering. Si/Ti ratios are commonly used as an indirect proxy of lake productivity, reflecting changes in biogenic silica input (e.g. Melles *et al.* 2012; Gjerde *et al.* 2017). Mn/Fe ratio indicate levels of anoxia, as Mn oxidises more rapidly than Fe leading to higher ratios under oxidising conditions (e.g. Naeher *et al.* 2013; Gjerde *et al.* 2017).

The first and second components of the PCA account for approximately 66% and 13% of the sample variance, respectively (Fig. 4). Component 1 scores accurately reproduce the stratigraphic units (Fig. 3).

Unit A (80-60 cm depth) – silty clay gyttja

At the base of the core, bedrock or boulders are overlain by firm, grey clay (~ 80-76 cm), which grades upwards to more organic, crudely stratified brown silty clay gyttja (Fig. 3). The upper part of the unit is abundant in bryophytes. This unit has low DBD (0.78 - 1.36, mean 1.02 g cm⁻³) and MS (8.30 – 47.10x10⁻⁵ χ_{hf} , mean 17.86x10⁻⁵ χ_{hf}), and high TOC (1.49-6.05, mean 2.69%). Mean grain sizes range from 17.42-32.41 μ m (fine silt and clay). Fluctuations in elemental composition (e.g. Ca, Ti) likely reflect variations in minerogenic sediment content. Si/Ti and Rb/Sr ratios remain high throughout this unit, while Ti/Al and Mn/Fe are low.

264

265 *Unit B (60-51 cm depth) – laminated silt and clay*

266 Unit B has a sharp contact with unit A and contains laminated grey clays and silts, with negligible
267 organic matter (Fig. 3). Laminations are <1-3 mm thick, with mean grain sizes of 11.53-30.57 μm . DBD
268 ($1.07 - 1.52$, mean 1.31 g cm^{-3}) and MS ($16.67 - 126.54 \times 10^{-5} \chi_{\text{hf}}$, mean $47.70 \times 10^{-5} \chi_{\text{hf}}$) values increase
269 sharply at the lower boundary, with the shift to minerogenic sediment. Ca and Ti concentrations are
270 high compared to the underlying more organic unit and decrease markedly at the upper boundary.
271 Low Si/Ti and Rb/Sr ratios and high Ti/Al and Mn/Fe ratios are consistent with low TOC values (0.43-
272 0.67, mean 0.54%) and are indicative of high minerogenic sediment input and greatly reduced
273 biological activity.

274

275 *Unit C (51-32 cm depth) – gyttja, silt, and clay*

276 This unit has a gradational lower contact, and grades upwards to faintly laminated brown gyttja, silt,
277 and clay, with fluctuating organic and minerogenic components (mean grain sizes 17.87-42.60 μm).
278 DBD ($0.80 - 1.26$, mean 0.96 g cm^{-3}), MS ($6.15 - 30.66 \times 10^{-5} \chi_{\text{hf}}$, mean $19.38 \times 10^{-5} \chi_{\text{hf}}$), and elemental
279 values (notably Ca, Al, Ti, and Si), are similar to Unit A (Fig. 3). High Si/Ti ratios and TOC (0.77-5.18,
280 mean 3.66%), as well as high Rb/Sr ratios, and low Ti/Al and Mn/Fe ratios, suggest limited detrital
281 sediment input and reduced bedrock weathering and erosion (Table 3).

282

283 *Unit D (32-23 cm depth) – laminated silt and clay*

284 The laminated grey silts and clays in Unit D record an abrupt shift in physical properties and elemental
285 composition, despite the gradational sedimentological contacts (Fig. 3). The unit has high DBD ($1.12 -$
286 1.73 , mean 1.33 g cm^{-3}) and low TOC (0.82-3.57, mean 1.47%). Ca, Ti, and MS ($27.19-127.12 \times 10^{-5} \chi_{\text{hf}}$,
287 mean $86.17 \times 10^{-5} \chi_{\text{hf}}$) increase markedly at the lower contact, and a decrease in Rb/Sr ratios, compared
288 to unit C, suggests enhanced input of weathered, minerogenic sediment.

289

Unit E (23-0 cm depth) – faintly laminated gyttja, silt, and clay

Unit E contains faintly laminated brown gyttja, silt, and clay (8.46-41.97 μm). Despite uniform sedimentology, geochemical measurements and ordination results (Fig. 3) identify three depositional phases, divided into sub-units E1, E2, and E3.

Subunit E1 (23-16 cm) coarsens upwards, and has relatively high DBD (1.10 – 1.23, mean 1.16 g cm^{-3}) and MS (51.89 – 136.28 $\times 10^{-5} \chi_{\text{hf}}$, mean 97.34 $\times 10^{-5} \chi_{\text{hf}}$), and low TOC (0.94 – 1.77, mean 1.39%). Ca and Mn/Fe values decrease sharply at the lower boundary and remain low throughout. Ti/Al and Rb/Sr ratios, as well as PCA component 1 scores (PC1), increase rapidly at the lower contact, before gradually decreasing.

E2 (16-12 cm), which broadly fines upwards, has high DBD (1.21 – 1.39, mean 1.32 g cm^{-3}), MS (82.08 – 229.33 $\times 10^{-5} \chi_{\text{hf}}$, mean 171.94 $\times 10^{-5} \chi_{\text{hf}}$), and low TOC (0.78 – 1.22, mean 0.92%). Through this subunit, Ti values reduce, Ca values increase, and Rb/Sr decreases considerably before increasing towards the upper contact. These elemental profiles are reflected in an increase in PC1 scores towards the top of the subunit.

Subunit E3 (12-0 cm) has relatively high DBD (1.04 – 1.32, mean 1.22 g cm^{-3}) and MS (52.23 – 141.73 χ_{hf} , mean 86.60 χ_{hf}). TOC (0.81 – 1.75, mean 1.24%) increases towards the top of the succession, while MS progressively decreases. Grain size, Ti, Ca, Si/Ti, and Rb/Sr values show little variation, but Ti/Al ratios gradually increase with height. These elemental profiles are also reflected in the stable PC1 scores.

Lake sediment X-Ray Diffraction and cluster analysis

The Madsen Lake sediments show a complex, but relatively uniform mineralogy throughout the succession, and a dominance of richterite, phlogopite, orthoclase, quartz, chamosite, and albite. The

samples share a common spectrum and clusters reflect variations in the relative abundance of the same suite of minerals. Cluster analysis identifies 14 different mineralogical clusters (Table 5; Fig. 3). When plotted against core stratigraphy, five distinct populations are apparent, which correspond to the sedimentary units A-E and to XRF data (Fig. 3). Importantly, clusters show that the mineralogical signatures of the laminated clay units (B and D) are distinct from the less minerogenic horizons (Units A and C). Unit E2 shares similar cluster assignments to the underlying clay units (B and D).

Chronology

The Madsen Lake chronology is constrained by four ^{14}C ages from plant macrofossils. Some units have not been directly dated, due to unsuitable material for ^{14}C analysis, and their age has been estimated using the age-depth model (Fig. 3). Dates are expressed as calibrated years before 1950 CE (Common Era; cal. a BP) unless otherwise stated. A sample from the base of Unit A (ZAC-4, 76.0-76.5 cm depth), close to the onset of lake sedimentation, is dated to 1740-1535 cal. a BP. Sample ZAC-3 from the base of Unit B (59.0-60.0 cm depth) yields an age of 1322-1276 cal. a BP, marking the onset of a laminated silt and clay depositional phase.

The presence of a sharp, potentially erosive, contact between Unit A and B (60 cm) is represented in the age-depth model as a hiatus. The inclusion of a hiatus increases the uncertainties for this section of the age-depth model, but age control provided by samples ZAC-4 and ZAC-3 means that palaeoenvironmental interpretations are unaffected. Two samples from Unit E yielded ages of 603-557 cal. a BP (sample ZAC-1, 6.0-7.0 cm depth) and 658-550 cal. a BP (sample ZAC-2, 11.0-12.0 cm depth). The overlapping calibrated age range of ZAC-1 and ZAC-2 is a product of the ^{14}C calibration curve plateau (Hallstatt plateau) and is not thought to reflect a true age inversion of the sample (Jacobsson *et al.* 2018). Above these dated horizons, the upper-most laminations remain horizontally bedded, but it cannot be ruled out that this part of the succession (i.e. 0.0-7.0 cm) has been truncated

due to poor recovery at the sediment-water interface. This cannot be tested with the current chronology, but it does not affect interpretations of the central portion of the core.

Modelled sediment accumulation rates for each unit, based on the age-depth model, are 0.29 mm a⁻¹ (Unit A), 0.37 mm a⁻¹ (Unit B), 0.64 mm a⁻¹ (Unit C), 0.72 mm a⁻¹ (Unit D), and 0.28 mm a⁻¹ (Unit E). However, given the variations in grain size, minerogenic content, and changes in dry bulk density within the units, alongside the evidence for a possible erosive contact between Units A and B, it is likely that rate has varied.

Discussion

Madsen Lake catchment history

Three phases of enhanced glacial activity, indicated by increased minerogenic sediment input, are recorded in the Madsen Lake succession. Two of these are recorded by distinct intervals of laminated clay and silt (Units B and D; Fig. 3) and a corresponding shift in geochemical characteristics. We interpret these units as evidence for a phase of glacial advance and retreat (contained within Unit B) followed by a period of readvance (Unit D). These phases are separated by a unit of lower minerogenic sediment content, representing conditions of reduced glacial activity (Unit C). A less marked reduction in minerogenic input (Unit E1), coupled with continuing low TOC levels, may be due to ice recession and/or reduced glacial erosion and sediment excavation. A third, shorter phase of enhanced glacial activity is identified by the geochemical record of Unit E2, followed by a transition towards the top of the succession to conditions with lower glacial sediment input to the lake.

These shifts in minerogenic and geochemical characteristics are consistent with other proglacial lake sediment records in Svalbard (Gjerde *et al.* 2017; de Wet *et al.* 2018) and Greenland (van der Bilt *et al.* 2018), where minerogenic horizons are characterised by reduced total organic

carbon content, and an increase in dry bulk density, magnetic susceptibility, and elements such as Fe, Ti, and Ca. Variations in the degree of development and thickness of glacial lake sediment laminations are common and reflect changes in the depositional environment. This includes sediment inputs into the basin, fluctuations in lake water depth which in turn control distance from lake sediment inputs, the development of thermal and density stratification, and the likelihood of reworking and homogenization of sediments by bioturbation and wave action (e.g. Zillén *et al.* 2003; Zolitschka *et al.* 2015).

The Madsen Lake depositional history is outlined below. Unit ages have been assigned as modelled ages from the age-depth model based on four ¹⁴C ages (ZAC-1 to ZAC-4). It is important to note that, although three phases of enhanced glacier activity are recorded between 1322-1276 cal. a BP (ZAC-3, 59.0-60.0 cm) and 658-550 cal. a BP (ZAC-2, 11.0-12.0 cm), only the base of unit B has been directly dated, and modelled ages are discussed with appropriate caution.

Prior to 1740-1535 cal. a BP, outlet glaciers from the eastern margins of Slettebreen coalesced and advanced beyond the lake basin, depositing a large suite of moraines at the margins of Slettedalen (Moraine Position 1, Fig. 1). Following ice retreat and exposure of the lake basin, sedimentation began at c. 1740-1535 cal. a BP (Unit A). Low and fluctuating minerogenic sediment inputs, low DBD, relatively increased TOC and Si/Ti ratios suggest that glacial sediment supply was low and that the ice margin was situated up valley, possibly close to the present-day ice margins.

A period of glacial advance into the lower catchment (c. 1350-1190 cal. a BP) is recorded by a sharp contact into the laminated silts and clays of Unit B, together with an increase in DBD and a decrease in TOC%. This unit is enhanced in Fe, Ti, and Ca (Fig. 3), which corresponds to the elemental composition of the sandstone clast samples (Table 4) and may indicate that the glacier advanced over a sandstone-rich band within the pelitic metasedimentary bedrock. This may also explain the decrease

in Rb/Sr ratios. Despite the erosive contact at the base of Unit B, the excellent preservation of laminations, with no evidence of deformation, suggests that ice did not advance across the lake basin at that time. Whilst it is possible that sediment can be preserved following overrunning by cold-based ice, as seen in some High-Arctic lake settings (McFarlin *et al.* 2018), we see little evidence for this in the Madsen Lake catchment, and it is likely that during the deposition of Unit B, the ice margin lay around Moraine Position 2. It is not possible to ascertain whether Unit B was deposited during glacial advance, stillstand, or recession, but this unit provides clear evidence for an enhanced period of glacial activity and sediment erosion and downstream transfer. The timing of this phase of glacial activity, during the Dark Ages Cooling Period, is consistent with evidence from other Arctic proglacial lake and moraine records, which indicate an advance at approximately 1000 cal. a BP, prior to the LIA (Jomelli *et al.* 2016; van der Bilt *et al.* 2018).

Following the deposition of Unit B, the reduction in minerogenic sediment content and elemental values, together with a rise in TOC concentrations and the rich bryophyte content of Unit C, indicate that ice has receded and environmental conditions around the lake have returned to those recorded in Bed A. This part of the succession is not directly dated, but the 20 cm-thick unit suggests a prolonged period of ice-free conditions in the lower catchment, rather than a temporary quiescent phase during dynamic ice retreat. Our age-depth model suggests that these conditions lasted from c. 1190 to 940 cal. a BP. It is likely that the ice margins were located close to their present-day positions on the flanks of the plateau, or at higher elevations, but further modelling of palaeo-glaciological behaviour is required to resolve this further.

A second phase of enhanced glacial activity is recorded from 940-825 cal. a BP (modelled age; Unit D), indicated by renewed minerogenic sediment delivery, reduced TOC% and Si/Ti ratio, and increased DBD and MS values. We interpret this as a readvance of the glacier towards the lake basin.

This is followed by a short period of reduced minerogenic sediment input (Unit E1), which does not correspond to an increase in TOC% or the Si/Ti ratio, unlike the conditions recorded in units A and C. Low Mn/Fe ratios indicate anoxic bottom conditions and thus reduced lake water circulation, while shifts in Ca and Rb/Sr indicate reduced chemical weathering. We interpret this as most likely due to a reduction in meltwater input and associated generation of bottom flows in the lake, possibly as a result of glacier retreat.

A third phase of enhanced glacial activity is recorded by unit E2, close to the onset of the LIA (modelled age c. 700-550 cal. a BP). High DBD, MS, Mn/Fe, and GSD90 values, coupled with low TOC and Rb/Sr ratios are indicative of enhanced detrital sediment inputs, associated chemical weathering, and increased lake water circulation during this period. Unlike Units B and D, this phase is not visible in the sedimentary record. However, using XRD cluster analysis it is possible to identify similarities between the mineralogical signature of this unit and the preceding glacially-derived sediments (Units B and D). This unit may therefore represent a more muted or short-lived cold oscillation involving ice readvance that has not been clearly recorded in the sedimentary characteristics. Alternatively, it may mark a phase of enhanced meltwater input due to glacier retreat, but its modelled age at the onset of the Little Ice Age is more consistent with a period of glacier growth. This highlights that in the High Arctic, even relatively low amplitude geochemical changes can be indicative of pronounced environmental change and emphasises the value of detailed geochemical measurements to reliably reconstruct glacial history.

Unit E3, at the top of the succession, displays fluctuating mineral composition and consistent PCA scores. TOC% remains low until the top 2cm of the unit, as do Rb/Sr ratios. Laminations remain intact, but it cannot be ruled out that this part of the core has been truncated. If the core is intact, the age-depth model indicates that this unit coincides with the coldest part of the LIA, in which case

the very low accumulation (0.28 mm a^{-1}) rate may indicate a period of prolonged or perennial lake ice cover, and therefore reduced or non-deposition of sediment (e.g. Levy *et al.* 2014).

Sediment geochemistry and mineralogy

Examination of the relationships between sediment characteristics, TOC, elemental and mineralogical composition (Fig. 3), provides detailed insights into glacier behaviour and downstream sediment transfer. The phases of glacially-derived sediment deposition are characterised by high DBD and MS, low TOC, and GSD90 values that are indicative of elevated clay content. Increased Ti and Ca content seen in the Madsen Lake succession have also been used elsewhere as indicators of enhanced glacial erosion of catchment bedrock (Bakke *et al.* 2009; de Wet *et al.* 2018). The Ti-TOC biplot (Fig. 5C), demonstrates that sediments with higher TOC concentrations are relatively depleted in Ti, while glacially-derived sediments contain negligible organic carbon.

During glacial depositional phases, low TOC values and Si/Ti ratios (Fig. 3) suggest a lake environment with high clastic sediment input and thus limited biological activity. This is likely due to an increase in the relative abundance of the finest sediment size fractions ($<50 \mu\text{m}$), evidenced by the low GSD90 scores, which have been shown to inhibit sunlight penetration of the water column, and greatly reduce biological processes (Slemmons *et al.* 2017). During these phases, high Ti/Al ratios (Fig. 5B) point to an increase in detrital sediment inputs. Low Rb/Sr ratios demonstrate that Rb is not profoundly influenced by glacier activity in the Madsen Lake catchment, even though in other catchments it has been associated with enhanced chemical weathering and detrital clays (Jin *et al.* 2001; Vasskog *et al.* 2011). Instead, Sr levels increase during glacial advance phases, and its covariance with Ca (Fig. 5A) indicates the simultaneous glacially-driven bedrock weathering of these elements, and delivery to the lake downstream. This is consistent with monitored observations from Glacier de Tsanfleuron, Switzerland, where Sr and Ca concentrations become progressively concentrated in downstream meltwater systems (Fairchild *et al.* 1994). Glacially comminuted Ca-rich grains are easily

dissolved and transported by low temperature meltwater river systems (Fairchild *et al.* 1994, 1999; Anderson *et al.* 2000; Adamson *et al.* 2014), which may also partly explain their elevated concentrations in Madsen Lake during periods of glacier activity. MS values increase abruptly at the onset of glacial sediment depositional phases (Units B and D) and remain elevated but highly variable in the uppermost part of the succession (Units E1-E3). Together with fluctuating DBD values this may reflect short-term variations in glacier activity, meltwater flows, lake ice cover, and therefore sediment source and delivery into the lake basin. This highlights the intricacy of the sedimentary signature in this part of the succession and the complex ways in which glacier behaviour is recorded in lake sediments.

Drivers of Late Holocene Arctic glacier behaviour

The first phase of glacial activity recorded in Madsen Lake (Unit B) is consistent with data from other parts of Greenland, which suggest a phase of enhanced glacier activity at c. 1000 cal. a BP, prior to the LIA, and broadly coincident with the Dark Ages Cold Period (e.g. Ljungqvist, 2010 and Table 1). Diatom assemblages from Raffles Sø, Scoresby Sund, suggest the onset of colder conditions and lake ice growth at 1800 cal. a BP (Cremer *et al.* 2001). This precedes the glacial signal recorded in Madsen Lake, but could represent the onset of Late Holocene climatic deterioration in east Greenland. In southeast Greenland, ¹⁰Be ages suggest that the southernmost part of the GrIS reached a maximum at 1510 a (Winsor *et al.* 2014). Lake sediments proximal to the Kulusuk glacier in southeast Greenland record a major advance at 1300 cal. a BP (Balascio *et al.* 2015), and sediments from the nearby Ymer Lake, Ammassalik, also record glacier regrowth at c. 1200 cal. a BP (van der Bilt *et al.* 2018).

The second glacial advance recorded in Madsen Lake (Unit D: c. 940-825 cal. a BP) is synchronous with evidence of glacial advance in Greenland and further afield (Fig. 6H) during the Medieval Climate Anomaly (MCA). Lake sediments in east Greenland show that Istorvet ice cap reached its maximum at c. 865 cal. a BP, remaining at this position until at least 355 cal. a BP (Lowell

et al. 2013; Lusas *et al.* 2017). Surface exposure ages from moraines on Scoresby Sund have dated recent advances of the Bregne ice cap to 740 a (Levy, *et al.* 2014), and to 780 - 310 a in Gurreholm Dal (Kelly *et al.* 2008). In West Greenland and Baffin Island, moraine successions recently dated with both ^{10}Be and ^{36}Cl have provided compelling evidence for glacier advances at 975, 885, and 800 a (Young *et al.* 2015; Jomelli, *et al.* 2016). As highlighted by Lowell *et al.* (2013), these pre-LIA advances are not unique to Greenland - records from Switzerland (Holzhauser *et al.* 2005), Canada (Luckman 1995) and Alaska (Wiles *et al.* 2008), also demonstrate pre-LIA and LIA glacier advances.

The continuation of low biological activity after this second advance indicates a prolonged climate downturn, similar to that recorded at Istorvet ice cap to the south (Lowell *et al.* 2013; Lusas *et al.* 2017). A third phase of enhanced glacial activity after 700 a in the Madsen Lake catchment is evident only in the geochemical record, and not the visual stratigraphy, and likely reflects changes in regional climate associated with onset of the LIA. As stated above, the highest part of the succession, close to the sediment-water interface, may be incomplete, but it is not possible to test this due to chronological constraints. The sediments are horizontally laminated and undisturbed, and if considered an intact record, may represent a period of inferred extensive ice cover on the lake, and/or cold conditions, impeding sediment delivery to the lake basin. These conditions – the coldest recorded in the Madsen Lake succession – are concordant with widespread regional evidence of cooling into the LIA.

Over the last 2000 years, regional variations in Arctic climate (PAGES 2k Consortium 2013) have been manifest as complex spatial patterns of ice advance and retreat, and regional climate has been modulated by local factors (e.g. Lusas *et al.* 2017). Arctic glacier behaviour is driven by summer temperature (during ablation season), which accounts for up to 90% of interannual mass balance variations (Koerner 2005). Significant increases in precipitation at around 1000 cal. a BP could have helped to force glacier advance in Zackenberg, however ice core records suggest little variation in

accumulation rates over the last 1800 years (Fig. 6E; Andersen *et al.* 2006). The Late-Holocene advances recorded at Madsen Lake are coincident with reduced Arctic temperatures (0.4 °C below present), recorded in high-resolution proxy records (Fig. 6B, C; PAGES 2k Consortium 2013) and reconstructed temperature decreases at NGRIP (up to 2.5 °C cooling) (Fig. 6D), suggesting large-scale climatic cooling. At present, the mechanisms responsible for pre-LIA glacier expansions in Greenland (Fig. 6H) are disputed. Reductions in solar irradiance and a period of persistent tropical volcanism, thought to have caused the onset of the LIA (Miller *et al.* 2012; Swingedouw *et al.* 2015), have been invoked as forcing mechanisms for some Greenlandic glacial advances (Young *et al.* 2015; Jomelli *et al.* 2016). However, the Slettebreen glacier advances occurred before the periods of reduced irradiance (900 cal. a BP) and volcanic activity (650 cal. a BP). Sediments from the East Greenland shelf have provided evidence for strengthening of cold polar waters and reductions in primary productivity from 1400 cal. a BP (Fig. 6F, G; Perner *et al.* 2015, 2016), and periods of enhanced sea ice in Prinz Josef Fjord, ~ 150 km southwest of Madsen Lake (Kolling *et al.* 2017) throughout the Neoglacial. Van der Bilt *et al.* (2018) propose a mechanism by which weakening of the Sub Polar Gyre caused a change in North Atlantic Oscillation phasing, leading to climatic conditions conducive for glacier growth in Greenland, but not in western Europe. However, at present, the direct climatic forcing of these pre-LIA glacier expansion remains unsolved. Results from Madsen Lake are part of a growing body of evidence for pre-LIA glacier advances in this part of the Arctic. Together this suggests that the palaeo-behaviour of Slettebreen is not dependant on local conditions, but instead part of a regional response. Our results highlight the importance of high-resolution sediment geochemical analysis, to identify rapid glacier advance-retreat phases, where geomorphological and stratigraphical records are fragmentary.

Conclusions

Detailed geochemical analysis of proglacial lake sediments close to Zackenberg, northeast Greenland reveals three phases of enhanced glacial activity, including two distinct episodes of ice advance, in the

last 2000 years. The first two phases occurred prior to the Little Ice Age (c. 1320-800 cal. a BP) and are close in age to the Dark Ages Cold Period and the Medieval Climate Anomaly. The third phase (c. 700 cal. a BP) representing a short-lived glacier oscillation is associated with the onset of the Little Ice Age. This is consistent with recent evidence of a period of Arctic glacier advance prior to the Little Ice Age.

The sub-millennial glacier fluctuations identified in the Madsen Lake succession are not preserved in the moraine record. Significantly, high-resolution, coupled XRF and XRD analysis has allowed us to identify a phase of glacial sediment input that cannot be distinguished by sedimentology alone. This highlights the importance of detailed geochemical analysis for reconstructing sub-millennial, Arctic glacier behaviour. In regions where dating control is scarce, geochemical analysis can be used to examine variations in glacially-driven sediment erosion and deposition patterns and develop meaningful interpretations in the context of regional climate proxy records.

Acknowledgements. - We would like to thank two anonymous reviewers for their comments on an earlier manuscript. DEMs were provided by the Polar Geospatial Center under NSF OPP awards 1043681, 1559691 and 1542736. Fieldwork was made possible through EU-INTERACT funding (grant agreement No. 262693) under the European Community's Seventh Framework Programme, Manchester Metropolitan University research funding, and Liverpool John Moores' ECR Fellowship funding. Thanks to Gary Miller who ran the XRD samples at Manchester Metropolitan University.

References

- Abermann, J., van As, D., Wacker, S. & Langley, K. 2017: Mountain glaciers vs Ice sheet in Greenland: learning from a new monitoring site in West Greenland. *EGU General Assembly Conference Abstracts* 19, 9445.
- Adamson, K. R., Woodward, J. C. & Hughes, P. D. 2014: Glacial crushing of limestone and the production of carbonate-rich silts in a Pleistocene glaciofluvial system: a potential source of loess in Southern Europe. *Geografiska Annaler: Series A, Physical Geography* 96, 339-356.

575 Andersen, K. K., Ditlevsen, P. D., Rasmussen, S. O., Clausen, H. B., Vinther, B. M., Johnsen, S. J. &
 576 Steffensen, J. P. 2006: Retrieving a common accumulation record from Greenland ice cores for
 577 the past 1800 years. *Journal of Geophysical Research: Atmospheres*, 111, D15106,
 578 doi:10.1029/2005JD006765.

579 Anderson, S. P., Drever, J. I., Frost, C.D. & Holden, P. 2000: Chemical weathering in the foreland of a
 580 retreating glacier. *Geochimica et Cosmochimica Acta* 64, 1173–1189.

581 Axford, Y., Levy, L. B., Kelly, M. A., Francis, D. R., Hall, B. L., Langdon, P. G. & Lowell, T. V. 2017: Timing
 582 and magnitude of early to middle Holocene warming in East Greenland inferred from
 583 chironomids. *Boreas* 46, 678-687.

584 Bakke, J., Lie, Ø., Heegaard, E., Dokken, T., Haug, G. H., Birks, H. H., Dulski, P. & Nilsen, T. 2009: Rapid
 585 oceanic and atmospheric changes during the Younger Dryas cold period. *Nature Geoscience* 2,
 586 202-205.

587 Bakke, J., Trachsel, M., Kvisvik, B.C., Nesje, A. & Lyså, A. 2013: Numerical analyses of a multi-proxy
 588 data set from a distal glacier-fed lake, Sørsendalsvatn, western Norway. *Quaternary Science*
 589 *Reviews* 73, 182-195.

590 Balascio, N. L., D'Andrea, W. J. & Bradley, R. S. 2015: Glacier response to North Atlantic climate
 591 variability during the Holocene. *Climate of the Past* 11, 1587-1598.

592 Bennike, O. 2002: Late Quaternary history of Washington Land, North Greenland. *Boreas* 31, 260-272.

593 Bennike, O. & Weidick, A. 2001: Late Quaternary history around Nioghalvfjærdsfjorden and
 594 Jøkelbugten, North-East Greenland. *Boreas* 30, 205-227.

595 Bennike, O. & Wagner, B. 2012: Deglaciation chronology, sea-level changes and environmental
 596 changes from Holocene lake sediments of Germania Havn Sø, Sabine Ø, northeast Greenland.
 597 *Quaternary Research* 78, 103-109.

598 Bjørk, A. A., Kjær, K. H., Korsgaard, N. J., Khan, S. A., Kjeldsen, K. K., Andresen, C. S., Box, J. E., Larsen,
 599 N. K. & Funder, S. 2012: An aerial view of 80 years of climate-related glacier fluctuations in
 600 southeast Greenland. *Nature Geoscience* 5, 427, doi:10.1038/ngeo1481.

601 Blaauw, M. & Christen, J. A. 2011: Flexible paleoclimate age-depth models using an autoregressive
 602 gamma process. *Bayesian Analysis* 6, 457-474.

603 Bliss, L. C. 1997: Arctic ecosystems of North America. In Wielgolaski, F. E. (ed.): *Polar and Alpine*
 604 *Tundra*, 551-683. Elsevier, Amsterdam.

605 Bolch, T., Sandberg Sørensen, L., Simonsen, S. B., Mölg, N., Machguth, H., Rastner, P. & Paul, F. 2013:
 606 Mass loss of Greenland's glaciers and ice caps 2003–2008 revealed from ICESat laser altimetry
 607 data. *Geophysical Research Letters* 40, 875-881.

608 Böning, C. W., Behrens, E., Biastoch, A., Getzlaff, K. & Bamber, J. L. 2016: Emerging impact of
609 Greenland meltwater on deepwater formation in the North Atlantic Ocean. *Nature Geoscience* 9,
610 523-527.

611 Bretz, J. H. 1935: Physiographic studies in east Greenland. *American Geographical Society* 18, 159-267.

612 Briner, J. P., Stewart, H. A. M., Young, N. E., Philipps, W. & Losee, S. 2010: Using proglacial-threshold
613 lakes to constrain fluctuations of the Jakobshavn Isbrae ice margin, western Greenland, during
614 the Holocene. *Quaternary Science Reviews* 29, 3861-3874.

615 Briner, J. P., Young, N. E., Thomas, E. K., Stewart, H. A. M., Losee, S. & Truex, S. 2011: Varve and
616 radiocarbon dating support the rapid advance of Jakobshavn Isbrae during the Little Ice Age.
617 *Quaternary Science Reviews* 30, 2476-2486.

618 Carr, J. R., Stokes, C. R. & Vieli, A. 2013: Recent progress in understanding marine-terminating Arctic
619 outlet glacier response to climatic and oceanic forcing: Twenty years of rapid change. *Progress in*
620 *Physical Geography* 37, 436-467.

621 Christiansen, H. H. & Humlum, O. 1993: Glacial history and periglacial landforms of the Zackenberg
622 area, northeast Greenland: preliminary results. *Geografisk Tidsskrift-Danish Journal of*
623 *Geography* 93, 19-29.

624 Christiansen, H. H., Sigsgaard, C., Humlum, O., Rasch, M. & Hansen, B. U. 2008: Permafrost and
625 periglacial geomorphology at Zackenberg. *Advances in Ecological Research* 40, 151-174.

626 Christoffersen, K. S., Amsinck, S. L., Landkildehus, F., Lauridsen, T. L. & Jeppesen, E. 2008: Lake flora
627 and fauna in relation to ice-melt, water temperature and chemistry at Zackenberg. *Advances in*
628 *Ecological Research* 40, 371-389.

629 Cremer, H., Wagner, B., Melles, M. & Hubberten, H. W. 2001: The postglacial environmental
630 development of Raffles Sø, East Greenland: inferences from a 10,000 year diatom record. *Journal*
631 *of Paleolimnology* 26, 67-87.

632 Dearing, J. 1999: Magnetic Susceptibility. In Walden, J., Oldfield, F. & Smith, J. P. (eds.): *Environmental*
633 *Magnetism: a Practical Guide. Technical Guide No. 6*, 35-62, Quaternary Research Association,
634 London.

635 Evans, J., Ó Cofaigh, C., Dowdeswell, J. A. & Wadhams, P. 2009: Marine geophysical evidence for
636 former expansion and flow of the Greenland Ice Sheet across the north-east Greenland
637 continental shelf. *Journal of Quaternary Science* 24, 279-293.

638 Fairchild, I. J., Bradby, L. & Spiro, B. 1994: Reactive carbonate in glacial systems: a preliminary synthesis
639 of its creation, dissolution and reincarnation. In Deynoux, M., Miller, J.M.G., Domack, E.W., Eyles,
640 N., Fairchild, I. J. & Young, G. M. (eds.): *Earth's glacial record – IGCP Project 260*, 176–192.
641 Cambridge University Press, Cambridge.

642 Fairchild, I. J., Killawee, J. A., Hubbard, B. & Dreybrodt, W. 1999: Interactions of calcareous suspended
643 sediment with glacial meltwater: a field test of dissolution behaviour. *Chemical Geology* 155,
644 243–263.

645 Filzmoser, P. & Varmuz, K. 2017: *Chemometrics: Multivariate Statistical Analysis in Chemometrics. R*
646 *package version 1.4.2.* <https://CRAN.R-project.org/package=chemometrics>.

647 Gilbert, G. L., Cable, S., Thiel, C., Christiansen, H. H. & Elberling, B. 2017: Cryostratigraphy,
648 sedimentology, and the late Quaternary evolution of the Zackenberg River delta, northeast
649 Greenland. *The Cryosphere* 11, 1265-1282, doi: 10.5194/tc-11-1265-2017.

650 Gjerde, M., Bakke, J., D'Andrea, W. J., Balascio, N. L., Bradley, R. S., Vasskog, K., Olafsdottir, S., Røthe,
651 T. O., Perren, B. B. & Hormes, A. 2017: Holocene multi-proxy environmental reconstruction from
652 Lake Hakluytvatnet, Amsterdamøya Island Svalbard (79.5° N). *Quaternary Science Reviews* 183,
653 164-176.

654 Hansen, B. U., Sigsgaard, C., Rasmussen, L., Cappelen, J., Hinkler, J., Mernild, S.H., Petersen, D.,
655 Tamstorf, M.P., Rasch, M. & Hasholt, B. 2008: Present-day climate at Zackenberg. *Advances in*
656 *Ecological Research* 40, 111-149.

657 Hansen, J., Topp-Jørgensen, E. & Christensen, T. R. 2015: *Zackenberg Ecological Research Operations*
658 *21st Annual Report*. 96 pp. Aarhus University, DCE – Danish Centre for Environment and Energy.

659 Hobbie, J. E., Shaver, G. R., Rastetter, E. B., Cherry, J. E., Goetz, S. J., Guay, K. C., Gould, W. A. & Kling,
660 G. W. 2017: Ecosystem responses to climate change at a Low Arctic and a High Arctic long-term
661 research site. *Ambio* 46, 160-173.

662 Holzhauser, H., Magny, M. & Zumbühl, H. J. 2005: Glacier and lake-level variations in west-central
663 Europe over the last 3500 years. *The Holocene* 15, 789-801.

664 Jacobsson, P., Hamilton, W. D., Cook, G., Crone, A., Dunbar, E., Kinch, H., Naysmith, P., Tripney, B. &
665 Xu, S. 2018: Refining the Hallstatt Plateau: Short-Term 14C Variability and Small Scale Offsets in
666 50 Consecutive Single Tree-Rings from Southwest Scotland Dendro-Dated to 510–460
667 BC. *Radiocarbon* 60, 219-237.

668 Jin, Z., Wang, S., Shen, J., Zhang, E., Li, F., Ji, J. & Lu, X. 2001: Chemical weathering since the Little Ice
669 Age recorded in lake sediments: a high-resolution proxy of past climates. *Earth Surface Processes*
670 *and Landforms* 26, 775–782.

671 Jomelli, V., Lane, T., Favier, V., Masson-Delmotte, V., Swingedouw, D., Rinterknecht, V.,
672 Schimmelpfennig, I., Brunstein, D., Verfaillie, D., Adamson, K. & Leanni, L. 2016: Paradoxical cold
673 conditions during the medieval climate anomaly in the Western Arctic. *Scientific Reports* 6,
674 32984, doi: 10.1038/srep32984.

675 Kelly, M. A. & Lowell, T. V. 2009: Fluctuations of local glaciers in Greenland during latest Pleistocene
676 and Holocene time. *Quaternary Science Reviews* 28, 2088-2106.

677 Kelly, M. A., Lowell, T. V., Hall, B. L., Schaefer, J. M., Finkel, R. C., Goehring, B. M., Alley, R. B. & Denton,
678 G. H. 2008: A ^{10}Be chronology of lateglacial and Holocene mountain glaciation in the Scoresby
679 Sund region, east Greenland: implications for seasonality during lateglacial time. *Quaternary*
680 *Science Reviews* 27, 2273-2282.

681 Klug, M., Bennike, O. & Wagner, B. 2009a: Repeated short-term bioproductivity changes in a coastal
682 lake on Store Koldewey, northeast Greenland: an indicator of varying sea-ice coverage? *The*
683 *Holocene* 19, 653-663.

684 Klug, M., Schmidt, S., Bennike, O., Heiri, O., Melles, M. & Wagner, B. 2009b: Lake sediments from store
685 Koldewey, northeast Greenland, as archive of late pleistocene and holocene climatic and
686 environmental changes. *Boreas* 38, 59-71.

687 Kobashi, T., Menviel, L., Jeltsch-Thömmes, A., Vinther, B. M., Box, J.E., Muscheler, R., Nakaegawa, T.,
688 Pfister, P.L., Döring, M., Leuenberger, M. & Wanner, H. 2017: Volcanic influence on centennial to
689 millennial Holocene Greenland temperature change. *Scientific Reports* 7, 1441, doi:
690 10.1038/s41598

691 Koerner, R. M. 2005: Mass balance of glaciers in the Queen Elizabeth Islands, Nunavut, Canada. *Annals*
692 *of Glaciology* 42, 417-423.

693 Kolling, H. M., Stein, R., Fahl, K., Perner, K. & Moros, M. 2017: Short-term variability in late Holocene
694 sea ice cover on the East Greenland Shelf and its driving mechanisms. *Palaeogeography,*
695 *Palaeoclimatology, Palaeoecology* 485, 336-350.

696 Lasher, G. E., Axford, Y., McFarlin, J. M., Kelly, M. A., Osterberg, E. C. & Berkelhammer, M. B. 2017:
697 Holocene temperatures and isotopes of precipitation in Northwest Greenland recorded in
698 lacustrine organic materials. *Quaternary Science Reviews* 170, 45-55.

699 Leeman, A., & Niessen, F. 1994: Holocene glacial activity and climate variations in the Swiss Alps:
700 reconstructing a continuous record from proglacial lake sediments. *The Holocene* 4, 259-268.

701 Levy, L. B., Kelly, M. A., Lowell, T. V., Hall, B. L., Hempel, L. A., Honsaker, W. M., Lusas, A. R., Howley,
702 J. A. & Axford, Y. L. 2014: Holocene fluctuations of Bregne ice cap, Scoresby Sund, east Greenland:
703 a proxy for climate along the Greenland Ice Sheet margin. *Quaternary Science Reviews* 92, 357-
704 368.

705 Ljungqvist, F. C. 2010: A new reconstruction of temperature variability in the extra-tropical Northern
706 Hemisphere during the last two millennia. *Geografiska Annaler: Series A, Physical Geography* 92,
707 339-351.

- Lloyd, J. M. 2006: Late Holocene environmental change in Disko Bugt, west Greenland: interaction between climate, ocean circulation and Jakobshavn Isbræ. *Boreas* 35, 35-49.
- Lowell, T. V., Hall, B. L., Kelly, M. A., Bennike, O., Lusas, A. R., Honsaker, W., Smith, C. A., Levy, L. B., Travis, S. & Denton, G. H. 2013: Late Holocene expansion of Istorvet ice cap, Liverpool Land, east Greenland. *Quaternary Science Reviews* 63, 128-140.
- Luckman, B. H. 1995: Calendar-dated, early 'Little Ice Age' glacier advance at Robson Glacier, British Columbia, Canada. *The Holocene* 5, 149-159.
- Lund, M., Abermann, J. & Skov, K. 2017: Environmental effects of a rare rain event in the high Arctic. *EGU General Assembly Conference Abstracts* 19, 9462.
- Lusas, A. R., Hall, B. L., Lowell, T. V., Kelly, M. A., Bennike, O., Levy, L. B. & Honsaker, W. 2017: Holocene climate and environmental history of East Greenland inferred from lake sediments. *Journal of Paleolimnology* 57, 321-341.
- MacGregor, K. R., Riihimäki, C. A., Myrbo, A., Shapley, M. D. & Jankowski, K. 2011: Geomorphic and climatic change over the past 12,900 yr at Swiftcurrent Lake, Glacier National Park, Montana, USA. *Quaternary Research* 75, 80-90.
- Machguth, H., Rastner, P., Bolch, T., Mölg, N., Sørensen, L. S., Aðalgeirsdóttir, G., Van Angelen, J. H., Van den Broeke, M. R. & Fettweis, X. 2013: The future sea-level rise contribution of Greenland's glaciers and ice caps. *Environmental Research Letters* 8, 025005. doi: 10.1088/17489326/8/2/025005.
- Machguth, H., Thomsen, H. H., Weidick, A., Ahlstrøm, A. P., Abermann, J., Andersen, M. L., Andersen, S.B., Bjørk, A. A., Box, J. E., Braithwaite, R. J. & Bøggild, C. E. 2016: Greenland surface mass-balance observations from the ice-sheet ablation area and local glaciers. *Journal of Glaciology* 62, 861-887.
- McFarlin, J. M., Axford, Y., Osburn, M. R., Kelly, M. A., Osterberg, E. C. and Farnsworth, L. B. 2018: Pronounced summer warming in northwest Greenland during the Holocene and Last Interglacial. *Proceedings of the National Academy of Sciences* 201720420, doi: 10.1073/pnas.1720420115
- Meier, M. F. and Post, A. 1969: What are glacier surges? *Canadian Journal of Earth Sciences* 6, 807-817.
- Melles, M., Brigham-Grette, J., Minyuk, P. S., Nowaczyk, N. R., Wennrich, V., DeConto, R. M., Anderson, P. M., Andreev, A. A., Coletti, A., Cook, T. L. & Haltia-Hovi, E. 2012: 2.8 million years of Arctic climate change from Lake El'gygytgyn, NE Russia. *Science* 337, 315-320 doi: 10.1126/science.1222135.

741 Miller, G. H., Geirsdóttir, Á., Zhong, Y., Larsen, D. J., Otto-Bliesner, B. L., Holland, M. M., Bailey, D. A.,
 742 Refsnider, K. A., Lehman, S. J., Southon, J. R. & Anderson, C. 2012: Abrupt onset of the Little Ice
 743 Age triggered by volcanism and sustained by sea-ice/ocean feedbacks. *Geophysical Research*
 744 *Letters* 39, L02708, doi: 10.1029/2011GL050168.

745 Moon, T., Joughin, I., Smith, B., Broeke, M. R., Berg, W. J., Noël, B. & Usher, M. 2014: Distinct patterns
 746 of seasonal Greenland glacier velocity. *Geophysical Research Letters* 41, 7209-7216.

747 Naeher, S., Gilli, A., North, R. P., Hamann, Y. & Schubert, C. J. 2013: Tracing bottom water oxygenation
 748 with sedimentary Mn/Fe ratios in Lake Zurich, Switzerland. *Chemical Geology* 352, 125-133.

749 Noël, B., van de Berg, W. J., Wessem, V., Melchior, J., Van Meijgaard, E., Van As, D., Lenaerts, J.,
 750 Lhermitte, S., Munneke, P. K., Smeets, C. J. P. and Van Uft, L. H. 2018: Modelling the climate and
 751 surface mass balance of polar ice sheets using RACMO2-Part 1: Greenland (1958-2016).
 752 *The Cryosphere* 12, 811-831.

753 Ó Cofaigh, C., Dowdeswell, J. A., Evans, J., Kenyon, N. H., Taylor, J., Mienert, J. & Wilken, M. 2004:
 754 Timing and significance of glacially influenced mass-wasting in the submarine channels of the
 755 Greenland Basin. *Marine Geology* 207, 39-54.

756 PAGES 2k Consortium 2013: Continental-scale temperature variability during the last two millennia.
 757 *Nature Geoscience* 6, 339–346.

758 Palmer, A., Rose, J., Lowe, J. J., & MacLeod, A. 2010: Annually resolved events of Younger Dryas
 759 glaciation in Lochaber (Glen Roy and Glen Spean), Western Scottish Highlands. *Journal of*
 760 *Quaternary Science* 25, 581-596.

761 Pedersen, M., Weng, W. L., Keulen, N. & Kokfelt, T. 2013: A new seamless digital 1: 500 000 scale
 762 geological map of Greenland. *Geological Survey of Denmark and Greenland* 28, 65-68.

763 Perner, K., Moros, M., Lloyd, J. M., Jansen, E. & Stein, R. 2015: Mid to late Holocene strengthening of
 764 the East Greenland Current linked to warm subsurface Atlantic water. *Quaternary Science*
 765 *Reviews* 129, 296-307.

766 Perner, K., Jennings, A. E., Moros, M., Andrews, J. T. & Wacker, L. 2016: Interaction between warm
 767 Atlantic-sourced waters and the East Greenland Current in northern Denmark Strait (68°N) during
 768 the last 10600 cal. a BP *Journal of Quaternary Science* 31, 472-483.

769 R Core Team. 2017: *R: A language and environment for statistical computing*. R Foundation for
 770 Statistical Computing, Vienna, Austria. <https://www.R-project.org/>.

771 Rastner, P., Bolch, T., Mölg, N., Machguth, H., Le Bris, R. & Paul, F. 2012: The first complete inventory
 772 of the local glaciers and ice caps on Greenland. *The Cryosphere* 6, 1483-1495.

773 Rea, B. R. 2009: Defining modern day Area-Altitude Balance Ratios (AABRs) and their use in glacier-
 774 climate reconstructions. *Quaternary Science Reviews* 28, 237-248.

775 Reimer, P. J., Bard, E., Bayliss, A., Beck, J. W., Blackwell, P. G., Ramsey, C. B., Buck, C. E., Cheng, H.,
 776 Edwards, R. L., Friedrich, M., Grootes, P. M., Guilderson T.P., Hafliðason H., Hajdas I., Hatte C.,
 777 Heaton T.J., Hoffmann D.L., Hogg A.G., Hughen K.A., Kaiser K.F., Kromer B., Manning S.W., Niu
 778 M., Reimer R.W., Richards D.A., Scott E.M., Southon J.R., Staff R.A., Turney C.S.M., van der Plicht
 779 J. 2013: IntCal13 and Marine13 radiocarbon age calibration curves 0–50,000 years cal
 780 BP. *Radiocarbon* 55, 1869-1887.

781 Schmidt, S., Wagner, B., Heiri, O., Klug, M., Bennike, O. & Melles, M. 2011: Chironomids as indicators
 782 of the Holocene climatic and environmental history of two lakes in northeast Greenland. *Boreas*
 783 40, 116-130.

784 Sharp, M., Lawson, W. & Anderson, R. S. 1988: Tectonic processes in a surge-type glacier. *Journal of*
 785 *Structural Geology* 10, 499-515.

786 Slemmons, K. E., Medford, A., Hall, B. L., Stone, J. R., McGowan, S., Lowell, T., Kelly, M. & Saros, J. E.
 787 2017: Changes in glacial meltwater alter algal communities in lakes of Scoresby Sund, Renland,
 788 East Greenland throughout the Holocene: Abrupt reorganizations began 1000 years before
 789 present. *The Holocene* 27, 929-940.

790 Striberger, J., Björck, S., Benediktsson, Í. Ö., Snowball, I., Uvo, C. B., Ingólfsson, Ó. & Kjær, K. H. 2011:
 791 Climatic control of the surge periodicity of an Icelandic outlet glacier. *Journal of Quaternary*
 792 *Science* 26, 561-565.

793 Swingedouw, D., Ortega, P., Mignot, J., Guilyardi, E., Masson-Delmotte, V., Butler, P. G., Khodri, M. &
 794 Séférian, R. 2015: Bidecadal North Atlantic ocean circulation variability controlled by timing of
 795 volcanic eruptions. *Nature Communications* 6, 6545. doi: 10.1038/ncomms7545.

796 Van der Bilt, W., Rea, B., Spagnolo, M., Roerdink, D., Jørgensen, S. & Bakke, J. 2018: Novel
 797 sedimentological fingerprints link shifting depositional processes to Holocene climate transitions
 798 in East Greenland. *Global and Planetary Change* 164, 52-64.

799 Vasskog, K., Nesje, A., Støren, E. N., Waldmann, N., Chapron, E. & Ariztegui, D. 2011: A Holocene record
 800 of snow-avalanche and flood activity reconstructed from a lacustrine sedimentary sequence in
 801 Oldevatnet, western Norway. *The Holocene* 21, 597-614.

802 Vieli, A., Lane, T. & Adamson, K. 2017: Long-term evolution of a small ice cap in Greenland: a dynamic
 803 perspective from numerical flow modelling. *EGU Geophysical Research Abstracts* 19, 12149.

804 Vinther, B. M., Jones, P. D., Briffa, K.R., Clausen, H. B., Andersen, K. K., Dahl-Jensen, D. & Johnsen, S.
 805 J. 2010: Climatic signals in multiple highly resolved stable isotope records from
 806 Greenland. *Quaternary Science Reviews* 29, 522-538.

- Wagner, B., Melles, M., Hahne, J., Niessen, F. & Hubberten, H. W. 2000: Holocene climate history of Geographical Society Ø, East Greenland—evidence from lake sediments. *Palaeogeography, Palaeoclimatology, Palaeoecology* 160, 45-68.
- Weidick, A. 1968: Observations on some Holocene glacier fluctuations in west Greenland. *Meddelelser om Grønland* 165, 1-202.
- Weidick, A., Bennike, O., Citterio, M. & Nørgaard-Pedersen, N. 2012: Neoglacial and historical glacier changes around Kangersuneq fjord in southern West Greenland. *Geological Survey of Denmark and Greenland* 27, 1-68.
- de Wet, G. A., Balascio, N. L., D'Andrea, W. J., Bakke, J., Bradley, R. S. & Perren, B. 2018: Holocene glacier activity reconstructed from proglacial lake Gjøavatnet on Amsterdamøya, NW Svalbard. *Quaternary Science Reviews* 183, 188-203.
- Wiles, G. C., Barclay, D. J., Calkin, P. E. & Lowell, T. V. 2008: Century to millennial-scale temperature variations for the last two thousand years indicated from glacial geologic records of Southern Alaska. *Global and Planetary Change* 60, 115-125.
- Winsor, K., Carlson, A. E. & Rood, D. H. 2014: 10Be dating of the Narsarsuaq moraine in southernmost Greenland: evidence for a late-Holocene ice advance exceeding the Little Ice Age maximum. *Quaternary Science Reviews* 98, 135-143.
- Wouters, B., Noël, B., Moholdt, G., Ligtenberg, S. & van den Broeke, M. 2017: Mass loss of the Greenland peripheral glaciers and ice caps from satellite altimetry. *EGU General Assembly Conference Abstracts* 19, 9829.
- Young, N. E., Briner, J. P., Stewart, H. A., Axford, Y., Csatho, B., Rood, D. H. & Finkel, R. C. 2011: Response of Jakobshavn Isbræ, Greenland, to Holocene climate change. *Geology* 39, 131-134.
- Young, N. E., Schweinsberg, A. D., Briner, J. P. & Schaefer, J. M. 2015: Glacier maxima in Baffin Bay during the Medieval Warm Period coeval with Norse settlement. *Science Advances* 1, 1500806, doi: 10.1126/sciadv.1500806.
- Zillén, L., Snowball, I., Sandgren, P. & Stanton, T. 2003: Occurrence of varved lake sediment sequences in Varmland, west central Sweden: lake characteristics, varve chronology and AMS radiocarbon dating. *Boreas* 32, 612-626.
- Zolitschka, B., Francus, P., Ojala, A. E. & Schimmelmann, A. 2015: Varves in lake sediments—a review. *Quaternary Science Reviews* 117, 1-41.

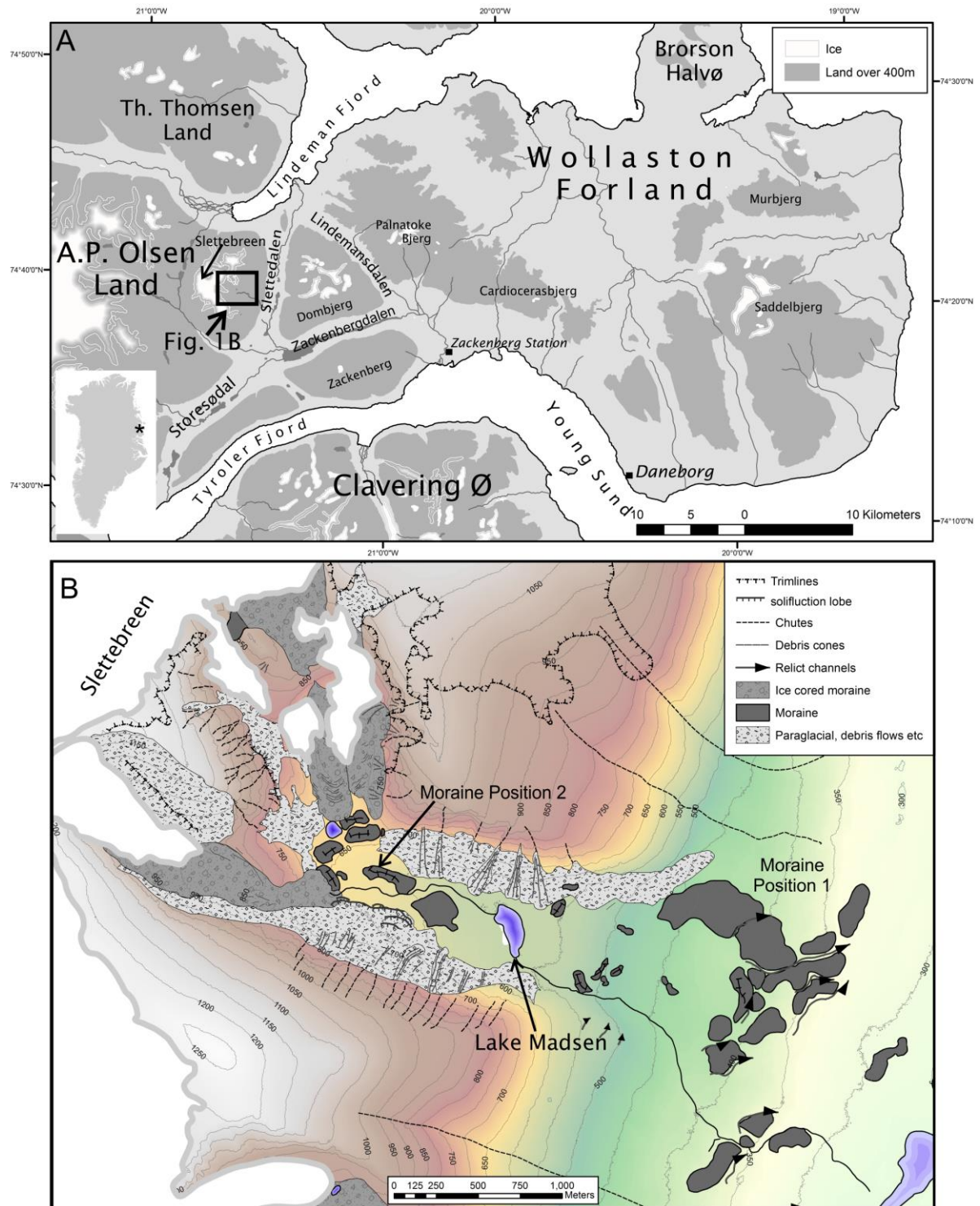


Figure 1. A. Map of A.P. Olsen Land and Wollaston Foreland areas, showing position of Slettebreen ice cap. B. Map of the Madsen Lake catchment, showing position of outlet glaciers from Slettebreen ice cap, moraines, and periglacial slope deposits. Moraine positions M1 and M2 are indicated – see text for discussion.

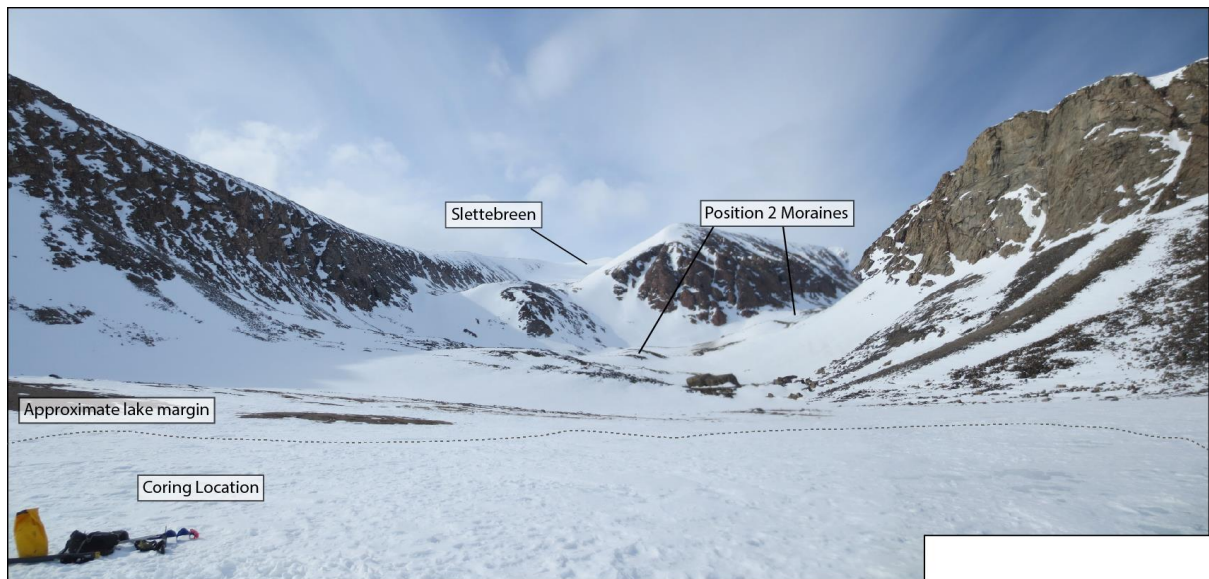


Figure 2. The Madsen Lake catchment. The margins of Slettebreen are out of view in the centre of the image. The steep valley sides and debris-covered slopes are visible beneath the snow cover. Note the ice drill and bag for scale.

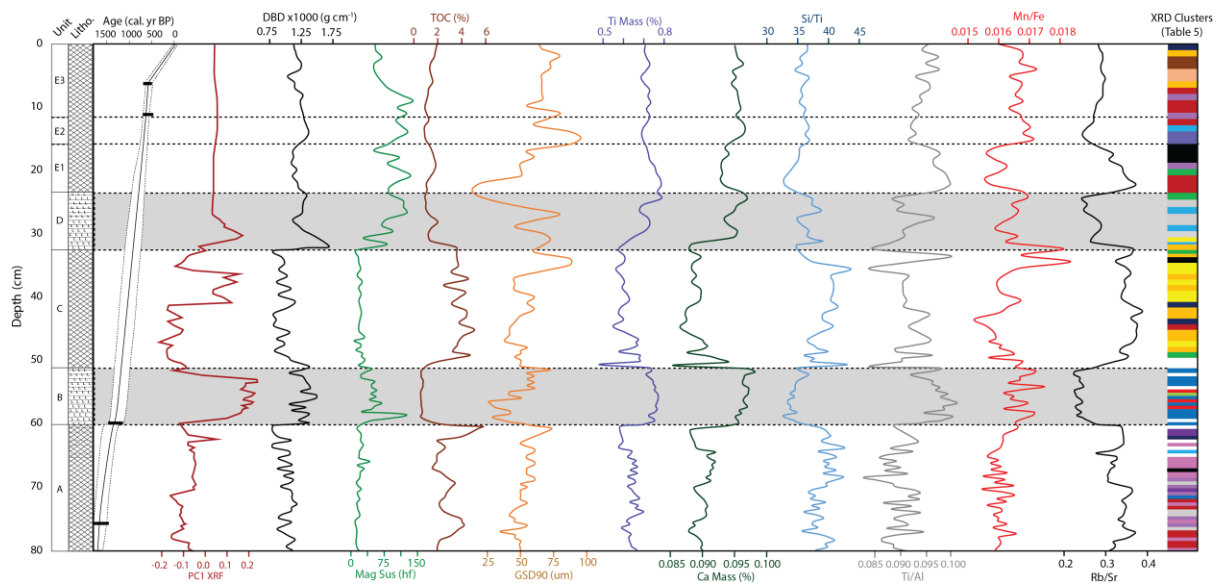


Figure 3. Physical and geochemical plot of the Madsen Lake sediment succession, including unit lithology following Troels Smith. Physical characteristics: Dry bulk density (DBD), Magnetic Susceptibility (Mag Sus), Total Organic Carbon (%), GSD90, and selected elemental compositions: Ti, Ca and ratios Si/Ti (an indirect indicator of lake productivity), Ti/Al (detrital sediment inputs), Mn/Fe (oxic vs anoxic conditions), and Rb/Sr (weathering). XRF PC1 scores are shown. XRD cluster assignments are indicated at the right of the geochemistry plot – see Table 5 for cluster composition

data. (For interpretation of the references to colour in this figure, the reader is referred to the web version of this article).

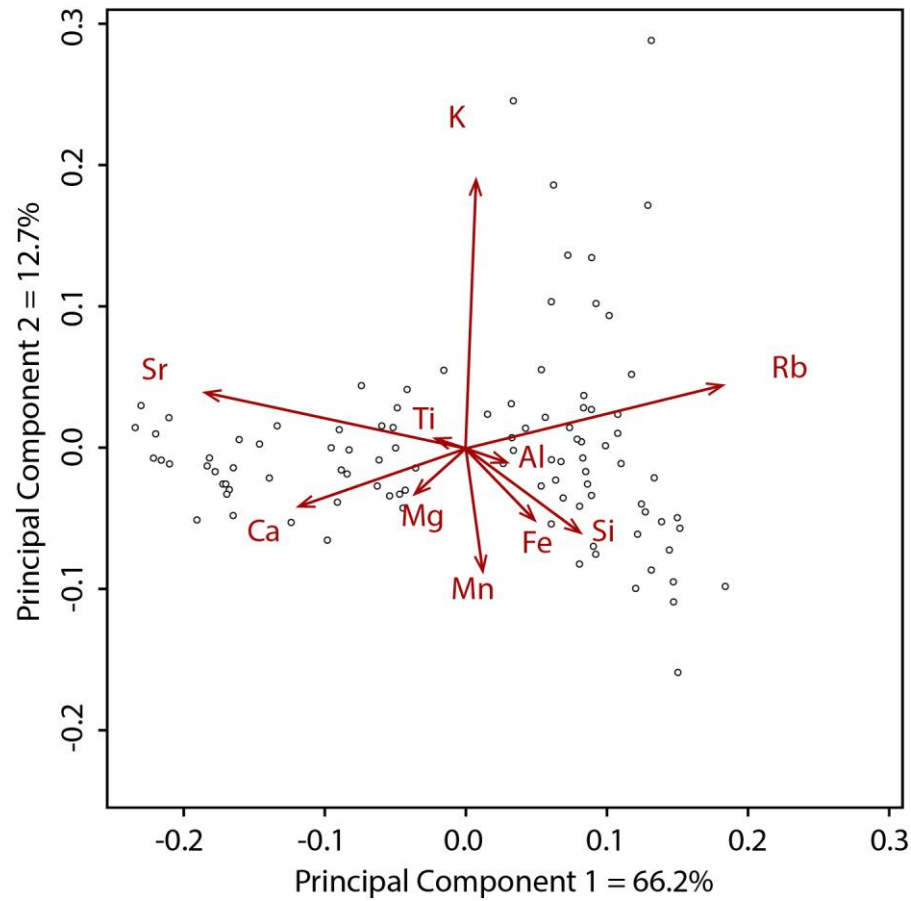


Figure 4. PCA plot of 10 elements (XRF analysis) selected on the basis of their abundance in the bedrock and lake sediments. Axis 1 accounts for approximately 66% of the sample variance. Axis 2 represents approximately 13% of the sample variance. Open circles represent each sampled horizon.

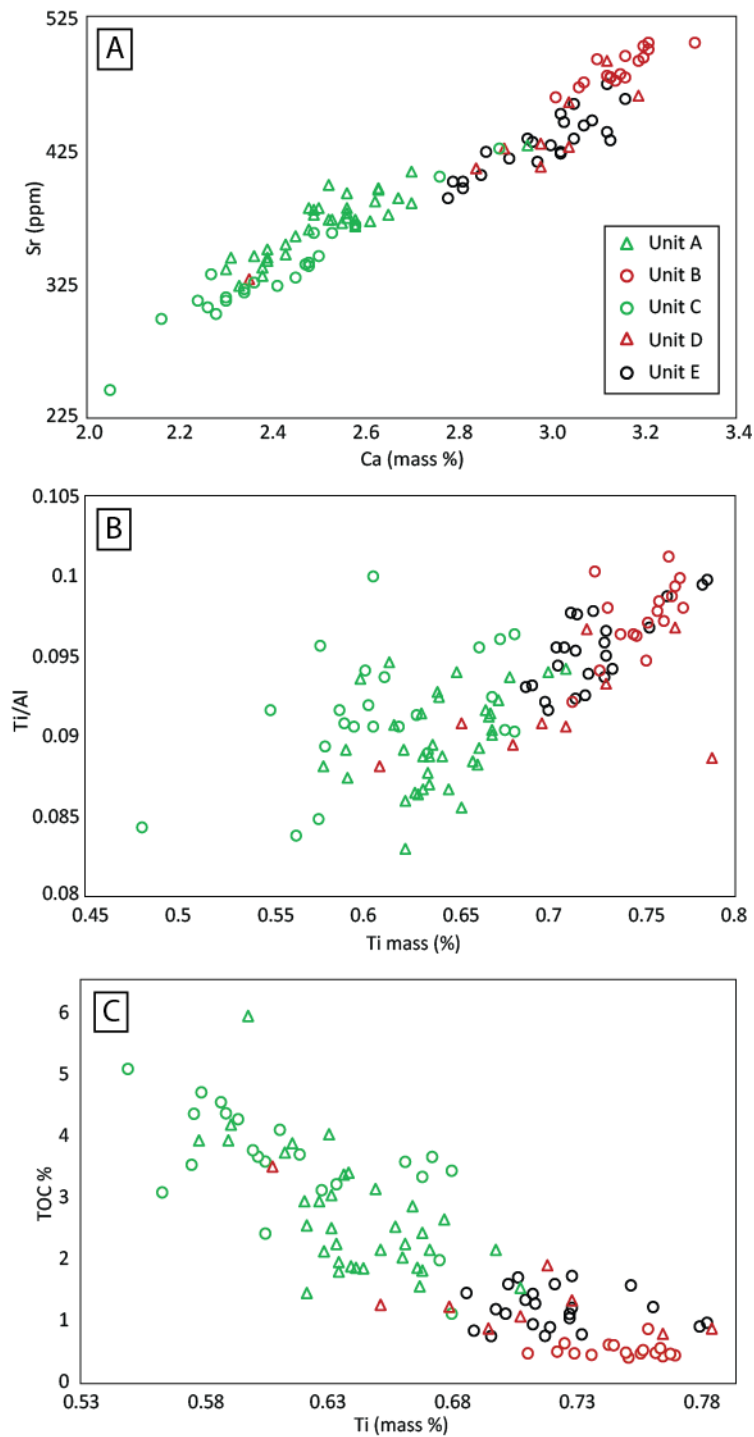


Figure 5. A. Scatterplot of Sr (ppm) vs Ca (mass %). More organic units, which represent reduced glacial input from Slettebreen are in green (Units A and C). Minerogenic units, which represent enhanced glacial activity are red (Units B and D). Unit E, which contains a complex minerogenic signal is in black; B. Relationship between Ti/Al and Ti (mass %). Sedimentary unit symbols follow Fig 5A. C. Relationship between TOC (%) and Ti (mass %). Sedimentary unit symbols follow Fig 5A (For interpretation of the references to colour in this figure legend, the reader is referred to the web version of this article).

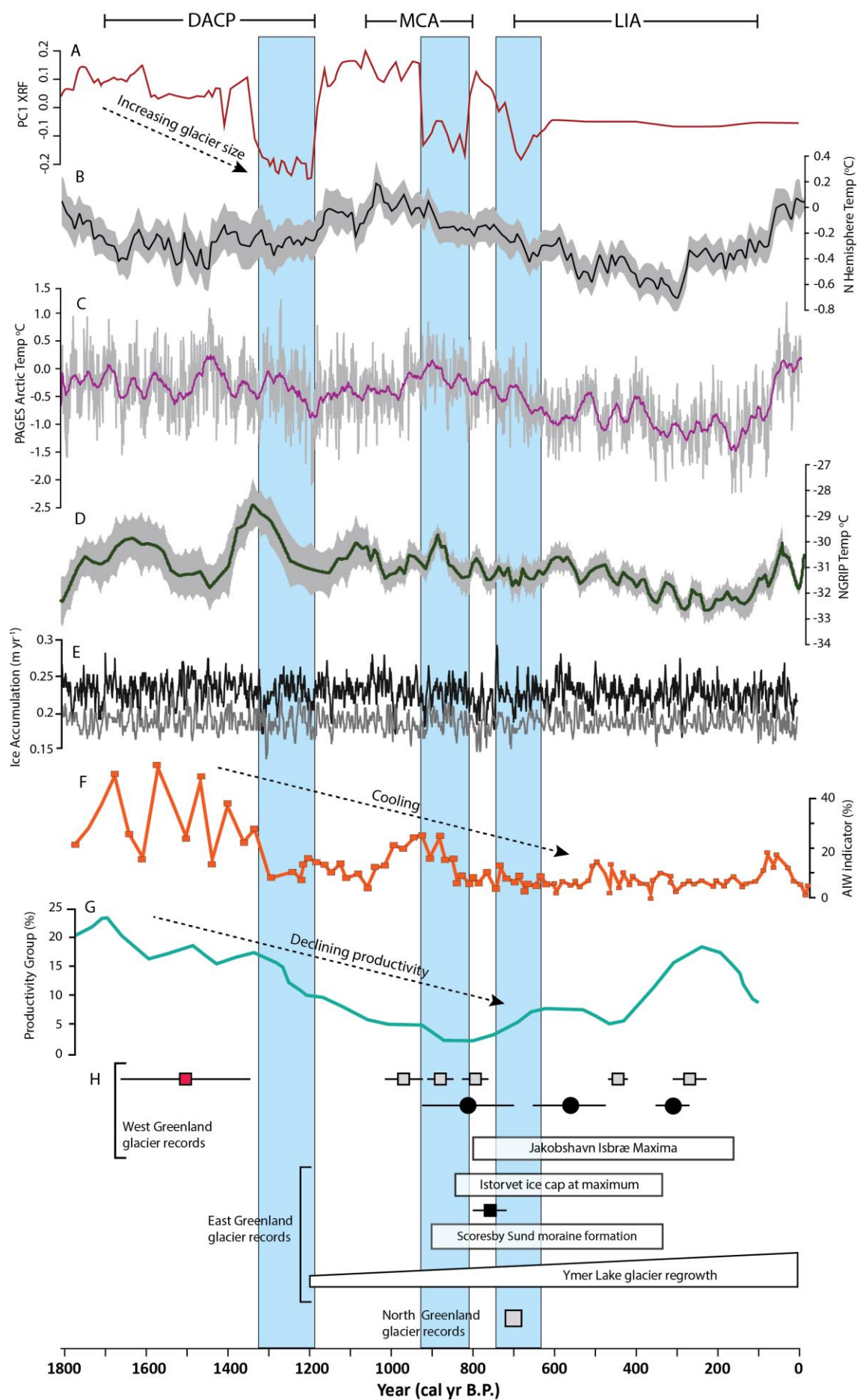


Figure 6. A. PC1 Axis from the Madsen Lake record. B. Extra-tropical Northern Hemisphere decadal mean temperature relative to the 1961-1990 instrumental temperature, with 2 standard deviation error bars (grey shading). C. Mean northern Hemisphere reconstructed temperature (PAGES 2k Network 2013). D. NGRIP reconstructed temperature from argon and nitrogen isotopes, with 2σ error bands (grey shading) (Kobashi *et al.* 2017). E. Ice accumulation records from GRIP (black line) and NGRIP (grey line) showing very limited variations in ice accumulation across the last 1800 years (Andersen *et al.*, 2011). F. Chilled Atlantic Water (AIW) foraminiferal assemblage group % from East Greenland Shelf (Perner *et al.* 2015). G. Foraminiferal assemblage productivity group % (Perner *et al.* 2016). H. Glacier records from West Greenland: Kiagtut Sermia, southwest Greenland (red square: Winsor *et al.* 2014), Uigordleq and Baffin Island (grey squares: Young *et al.* 2015), Disko Island (black circles: Jomelli *et al.* 2016), Jakobshavn Isbræ (Lloyd 2006; Briner *et al.* 2011; Young *et al.* 2011); East Greenland: Istorvet ice cap (Lowell *et al.* 2013; Lusas *et al.* 2017), Scoresby Sund (Kelly *et al.* 2008), Bregne Ice Cap (black square: Levy *et al.* 2014), Ymer Lake, Ammassalik (Van der Bilt *et al.* 2018); and North Greenland (Bennike 2002). Specific climatic periods/events are shown at the top: Dark Ages Cold Period (DACP), Medieval Climate Anomaly (MCA) and Little Ice Age (LIA) (after Kolling *et al.* 2017). Periods of glacier advance inferred from PCA axis 1 are shown in vertical blue bars (For interpretation of the references to colour in this figure legend, the reader is referred to the web version of this article).

Ice mass	Sedimentary record	Dating method	Age	Advance/ Max/Retreat	Author
West Greenland					
Uigordleq lake valley	Moraine	¹⁰ Be	820 a	Maximum	Young <i>et al.</i> (2015)
Jakobshavn Isbræ	Marine core	¹⁴ C	310-450 cal. a BP 100 cal. a BP	Advance Maximum	Briner <i>et al.</i> (2010, 2011); Young <i>et al.</i> (2011)
Qamanaarssup Sermia	Moraine	Historical	250-350 a 150 a	Advance Maximum	Weidick <i>et al.</i> (2012)
Kangiata Nunaata Sermia	Lake sediment	¹⁴ C	1650 cal. a BP	Advance	Weidick <i>et al.</i> (2012)
Kiagtut Sermia	Moraine	¹⁰ Be	1460 ± 110 a	Maximum	Winsor <i>et al.</i> (2014)
North Greenland					
Humboldt Glacier	Moraine	¹⁴ C	650 cal. a BP	Advance	Bennike (2002)
East Greenland					
Gurrenholm Dal glacier	Moraine	¹⁰ Be	249-749 a	Maximum	Kelly <i>et al.</i> (2008)
Bregne ice cap	Moraine	¹⁰ Be	740–9,600 a	Maximum	Levy <i>et al.</i> (2014)
Istorvet ice cap	Moraine and lake sediment	¹⁴ C	800 cal. a BP 290 cal. a BP	Advance Retreat	Lowell <i>et al.</i> (2013)
South Greenland					
Kulusuk lake	Lake sediment	¹⁴ C and ²¹⁰ Pb	From 4100 cal. a BP	Fluctuations	Balascio <i>et al.</i> (2015)

Table 1. Records of Late Holocene (5 ka to present) glacier activity in Greenland, including proglacial lake and moraine sediment archives.

Sample number	Beta code	Core depth (cm)	Sample material	Sample mass (mg)	¹⁴ C age a BP	Error +/- (1 σ)	Age (cal. a BP, 2 σ)	Calendar age (CE)	Δ ¹³ C
ZAC-1	466979	6.0-7.0	Plant	2.60	620	30	658 - 550	1292 - 1400	-26.3
ZAC-2	469962	11.0-12.0	Plant	0.93	660	30	603 - 557 674 - 628	1347 - 1393 1276 - 1322	-29.5
ZAC-3	469963	59.0-60.0	Plant	1.00	1390	30	1348 - 1276	602 - 674	-25.1
ZAC-4	480589	76.0-76.5	Plant	0.52	1730	50	1740 - 1535	210 - 415	-23.8

Table 2. Radiocarbon ages of plant macrofossil samples (ZAC-1 to ZAC-4), calibrated using the Intcal13 curve. Calendar ages are displayed for comparison with climate records. All samples were prepared and analysed at Beta Analytic.

Unit	Acc. Rate (mm yr ⁻¹)	Mean grain size (μm)				Total Organic Carbon (%)				Dry bulk density (g cm ⁻³)				Magnetic susceptibility (hf)			
		Min	Max	Mean	Std.	Min	Max	Mean	Std.	Min	Max	Mean	Std.	Min	Max	Mean	Std.
E3		25.97	33.72	30.23	2.19	0.81	1.75	1.24	0.28	1.04	1.32	1.22	0.07	52.23	141.73	86.60	30.54
<i>E2</i>	0.28	<i>26.32</i>	<i>41.97</i>	<i>26.32</i>	<i>5.75</i>	<i>0.78</i>	<i>1.22</i>	<i>0.92</i>	<i>0.19</i>	<i>1.21</i>	<i>1.39</i>	<i>1.32</i>	<i>0.06</i>	<i>82.08</i>	<i>229.33</i>	<i>171.94</i>	<i>63.31</i>
E1		8.46	26.45	21.54	6.33	0.94	1.77	1.39	0.30	1.10	1.23	1.16	0.04	51.89	136.28	97.34	24.85
<i>D</i>	<i>0.72</i>	<i>9.61</i>	<i>38.17</i>	<i>25.11</i>	<i>8.97</i>	<i>0.82</i>	<i>3.57</i>	<i>1.47</i>	<i>0.81</i>	<i>1.12</i>	<i>1.73</i>	<i>1.33</i>	<i>0.16</i>	<i>27.19</i>	<i>127.12</i>	<i>86.17</i>	<i>28.78</i>
C	0.64	17.87	42.60	23.59	6.15	0.77	5.18	3.66	1.24	0.80	1.26	0.96	0.12	6.15	30.66	19.38	6.01
<i>B</i>	<i>0.37</i>	<i>11.53</i>	<i>30.57</i>	<i>21.74</i>	<i>5.67</i>	<i>0.43</i>	<i>0.67</i>	<i>0.54</i>	<i>0.08</i>	<i>1.07</i>	<i>1.52</i>	<i>1.31</i>	<i>0.13</i>	<i>16.67</i>	<i>126.54</i>	<i>47.70</i>	<i>24.16</i>
A	0.29	17.42	32.41	23.21	2.98	1.49	6.05	2.69	1.10	0.78	1.36	1.02	0.13	8.30	47.10	17.86	8.16

Table 3. Sediment characteristics of the Madsen Lake sequence with minimum, maximum, mean, and standard deviation values. Horizons B, D, and E2, associated with enhanced glacier activity, are indicated in italics.

Elemental composition (mass %)								
Lithology	Si	Al	Ca	K	Fe	Na	Mg	Ti
Sandstone	22.40	7.22	7.35	0.21	9.74	2.60	1.72	1.28
Gneiss	27.30	5.99	1.46	3.24	2.65	2.89	0.73	0.32
Gneiss	26.80	6.70	2.82	3.20	3.12	2.43	0.89	0.49
Unakite	32.00	6.33	4.35	2.30	2.21	2.15	0.39	0.21
Granite	23.40	6.88	5.13	3.93	6.69	1.76	2.25	0.52
Granite	27.90	6.37	0.57	3.96	2.27	2.86	0.55	0.29
Granite	26.00	6.48	5.28	0.82	4.18	2.90	2.64	0.20
Quartz	27.30	7.77	0.13	8.83	0.03	1.61	0.05	0.01

Table 4. Lithology and elemental composition (XRF, eight most abundant elements, mass %) of clast samples from the study region around Madsen Lake and Slettedalen. See text for further details of less abundant elements.


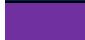











Cluster		Composition of dominant minerals (%)					
Colour, #		Richterite	Phlogopite	Orthoclase	Quartz	Chamosite	Albite
	1	22.0	28.5	18.0	15.0	10.5	6.0
	2	25.0	23.0	25.0	6.0	12.0	9.0
	3	31.0	29.0	26.0	3.0	6.0	5.0
	4	17.0	26.0	16.0	23.0	14.0	4.0
	5	22.0	19.5	23.0	19.0	11.5	5.0
	6	19.0	16.0	17.0	22.0	23.0	3.0
	7	30.0	21.0	25.0	7.0	11.0	6.0
	8	25.0	20.0	29.0	8.0	10.0	8.0
	9	18.0	22.0	20.0	14.0	23.0	3.0
	10	26.5	25.0	22.5	7.0	10.0	9.0
	11	19.0	26.5	19.0	21.0	11.5	3.0
	12	23.0	12.0	21.0	22.0	18.0	4.0
	13	18.0	33.0	15.0	15.0	14.0	5.0
	14	22.0	25.5	16.5	11.0	18.0	7.0

Table 5. Relative abundance of the dominant minerals present within the 14 Lake Madsen XRD clusters (see Fig. 3 for down-core cluster assignments) based on the relative intensity of diffraction peaks, which are indicative of crystalline concentrations.